Multiple pathways guide oxygen diffusion into flavoenzyme active sites

Riccardo Baron[a,b,1], Conor Riley[a,2], Pirom Chenprakhon[c,d,2], Kittisak Thotsaporn[c,3], Remko T. Winter[e,3], Andrea Alfieri[f], Federico Forneris[f], Willem J. H. van Berkel[g], Pimchai Chaiyen[c], Marco W. Fraaije[e], Andrea Mattevi[f,1], and J. Andrew McCammon[a,b,h,i]

Department of [a]Chemistry and Biochemistry and [h]Pharmacology, [b]Center for Theoretical Biological Physics, and [i]Howard Hughes Medical Institute, University of California at San Diego, La Jolla, CA 92093-0365; [c]Department of Biochemistry and Center for Excellence in Protein Structure and Function, Faculty of Science, and [d]Institute for Innovative Learning, Mahidol University, Rama 6 Road, Bangkok 10400, Thailand; [e]Laboratory of Biochemistry, Groningen Biomolecular Sciences and Biotechnology Institute, University of Groningen, Nijenborgh 4, 9747 AG Groningen, The Netherlands; [f]Department of Genetics and Microbiology, University of Pavia, Via Ferrata 1, 27100 Pavia, Italy; and [g]Laboratory of Biochemistry, Wageningen University, Dreijenlaan 3, 6703 HA Wageningen, The Netherlands

Edited by William A. Eaton, National Institutes of Health, Bethesda, MD, and approved April 29, 2009 (received for review April 6, 2009)

Dioxygen (O_2) and other gas molecules have a fundamental role in a variety of enzymatic reactions. However, it is only poorly understood which O_2 uptake mechanism enzymes employ to promote efficient catalysis and how general this is. We investigated O_2 diffusion pathways into monooxygenase and oxidase flavoenzymes, using an integrated computational and experimental approach. Enhanced-statistics molecular dynamics simulations reveal spontaneous protein-guided O_2 diffusion from the bulk solvent to preorganized protein cavities. The predicted protein-guided diffusion paths and the importance of key cavity residues for oxygen diffusion were verified by combining site-directed mutagenesis, rapid kinetics experiments, and high-resolution X-ray structures. This study indicates that monooxygenase and oxidase flavoenzymes employ multiple funnel-shaped diffusion pathways to absorb O_2 from the solvent and direct it to the reacting C4a atom of the flavin cofactor. The difference in O_2 reactivity among dehydrogenases, monooxygenases, and oxidases ultimately resides in the fine modulation of the local environment embedding the reactive locus of the flavin.

computational biochemistry | enzymology | flavin | oxygen reactivity

Dioxygen (O_2) and other gas molecules have a fundamental role in a variety of enzymatic reactions carried out in living organisms. Oxygen-using enzymes usually have kinetic rates many folds higher than those attained by artificial catalysts (1–4). One crucial unsolved question concerns how these small gas molecules reach their active sites in an effective manner. Former studies supported the general model of passive diffusion through proteins (5, 6). However, it was more recently proposed that O_2 preferentially follows highly specific tunnels to reach the core of protein matrices (7–13). Is it possible to generalize these features for different classes of enzymes? Do proteins preferentially employ single specific pathways or a multitude of routes to optimize the O_2 uptake process?

Pioneering studies on gas-diffusion in biomolecular systems focused on single diffusion pathways in proteins of the globin family (2, 14). For example, myoglobin served as an ideal test system for the first computational studies on gaseous reactants (14). Fluorescence-quenching experiments were used to correlate the diffusion behavior with solvent properties, e.g., viscosity (15, 16). Reaction intermediates of small gas molecules can be trapped in X-ray enzyme structures in limited favorable cases (17, 18) whereas time-resolved X-ray crystallography provides single-molecule-averaged insight (19). A general observation emerging from recent engineering studies of an O_2 transport protein is that design efforts based on static-structure models fail to address the molecular complexity critical for function (20). Thus, complementing experimental and computational approaches can improve our understanding of these dynamic processes at the atomic-level scale (7, 8, 21–25). However, no molecular dynamics (MD) study to date reported on the spontaneous, nonbiased diffusion of O_2 molecules from the bulk solvent to the active site of a flavoenzyme.

Flavoenzymes catalyze a wide range of reactions essential for maintaining cellular processes. Their striking chemical versatility is largely based on their ability to control the reaction of a flavin cofactor with O_2. Three major groups of flavoenzymes can be distinguished (3, 26, 27). First, the dehydrogenases, that are characterized by poor or no reactivity with oxygen. Second, the monooxygenases, that react very fast with O_2, forming a flavin adduct intermediate (C4a-hydroperoxyflavin; Scheme 1 and Fig. S1), which subsequently inserts an oxygen atom into the substrate molecule. Third, the oxidases, that catalyze a rapid 2-electron transfer to O_2 to produce H_2O_2, typically—but not always (28)—with no detectable catalytic intermediates. The reaction of reduced flavins with O_2 proceeds through an electron-transfer step that generates a caged radical pair, which is generally thought to be rate limiting. Reduced flavoprotein monooxygenases and oxidases typically react very rapidly with O_2, exhibiting bimolecular rate constants (up to 10^6 $M^{-1}{\cdot}s^{-1}$) that are close to a diffusion-controlled rate.

The biochemical and structural basis of the ability of flavoenzymes to react with O_2 remains to a large extent poorly understood, representing a most fascinating issue in flavoenzymology (3, 26). A key requirement for monooxygenases is that O_2 reaches the flavin to promote the catalyzed reaction through a C4a covalent adduct (3, 26, 27) (Scheme 1). However, only little is known about how oxidases react with O_2. A direct contact between the oxidase flavin and O_2 may not be necessary, leaving open the possibility that the enzymes of this class may react by tunneling pathways (24, 29) or electron transfer processes similar to what was reported for heme-containing enzymes (30).

Here, we investigate O_2 diffusion in the monooxygenase component (C_2) of *p*-hydroxyphenylacetate hydroxylase from *Acinetobacter baumannii* (31) and alditol oxidase (AldO) from *Streptomyces coelicolor* A3 (2) (32) using an integrated computational and experimental procedure. Enhanced-statistics MD

Author contributions: R.B., P. Chaiyen, M.W.F., and A.M. designed research; R.B., P. Chenprakhon, K.T., and R.T.W. performed research; R.B. and J.A.M. contributed new reagents/analytic tools; R.B., C.R., A.A., F.F., W.J.H.v.B. P. Chaiyen, M.W.F., A.M., and J.A.M. analyzed data; and R.B. and A.M. wrote the paper.

The authors declare no conflict of interest.

This article is a PNAS Direct Submission.

Freely available online through the PNAS open access option.

[1]To whom correspondence should be addressed. E-mail: rbaron@mccammon.ucsd.edu or mattevi@ipvgen.unipv.it.

[2]C.R. and P. Chenprakhon contributed equally to this work.

[3]K.T. and R.T.W. contributed equally to this work.

This article contains supporting information online at www.pnas.org/cgi/content/full/0903809106/DCSupplemental.

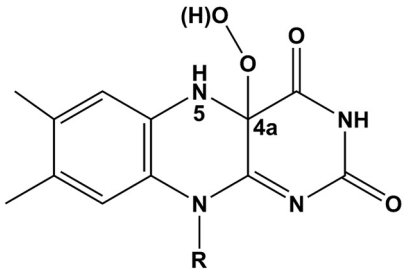

Scheme 1. Chemical formula of the C4a-hydroperoxyflavin molecule. The N5 and C4a atoms are labeled. The flavin is facing the viewer with its *re*-side (the *si*-side is on the opposite side).

simulations capture the spontaneous (unbiased) diffusion of O_2, filling the gap between current sampling times in protein simulations with explicit solvent ($\approx 10^1$ ns scale) (33, 34) and measured diffusion times (>10 ns scale). Our theoretical predictions were followed by experimental verification through site-directed mutagenesis, rapid kinetics measurements, and structural analysis of the C_2 and AldO enzymes. This integrated approach indicates that O_2 diffusion into both the monooxygenase and the oxidase flavoenzymes is effectively guided by multiple-pathways funnels that lead to defined O_2 entry points of active sites. Our data provide structural insight into the mechanism of O_2 uptake by flavoenzymes, emphasizing the importance of the protein microenvironment of the flavin in modulating oxygen reactivity.

Results

Oxygen Diffusion into C_2. We investigated the diffusion of O_2 molecules into the active site of C_2. Enhanced-statistics MD simulations were initialized based on the X-ray structure (2.8 Å resolution) of the enzyme bound to reduced FMN ($FMNH^-$) (31) and extended for 30 ns of overall enhanced time (Table S1). Out of a total of 500 O_2 trajectories at 300 K, we observe 4 complete spontaneous diffusion pathways that bring O_2 molecules in front of the *re*-side of $FMNH^-$ (Fig. 1) starting from

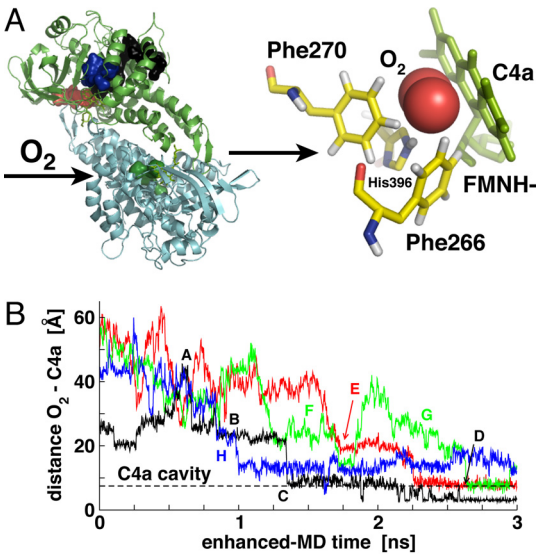

Fig. 1. O_2 spontaneous diffusion into C_2. (*A*) Four complete paths are observed from simulations at 300 K (volume isosurfaces) (*Left*). All paths conduct O_2 molecules (red spheres) (*Right*) to the *re*-side of the $FMNH^-$ (reduced flavin cofactor, green sticks) in close contact with its C4a carbon (*Right*). (*B*) Time series of the O_2 – C4a distance for the successful diffusion paths and key steps (see text). The dashed horizontal line defines the C4a flavin oxygen cavity.

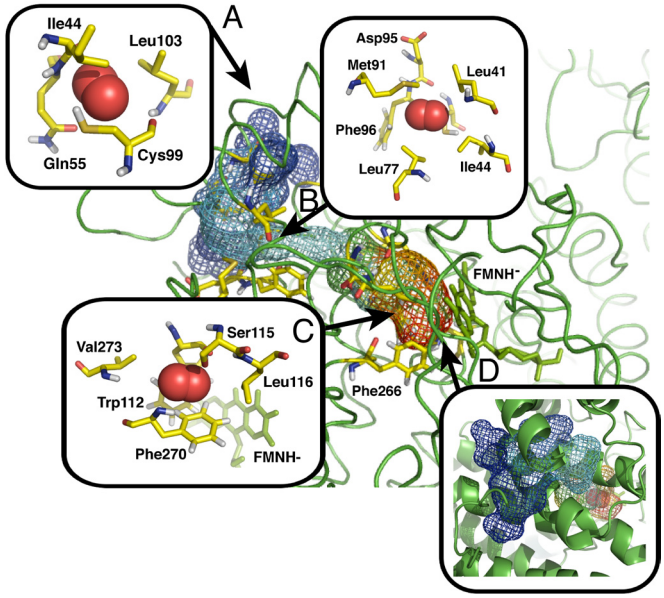

Fig. 2. Side-chain flexibility assists O_2 diffusion. Key steps along an example diffusion path for C_2. (*A*) Entrance into surface cavity. (*B*) Transport to an internal cavity. (*C*) Side-chain fluctuation mechanism. (*D*) Final entrance into the C4a preorganized cavity [overall tunnel view; volume isosurface is colored depending on simulation time from blue (entrance into the protein) to red (end of successful path)]. Snapshots refer to Fig. 1*B*, black line. See Movie S1 for a corresponding video clip.

random configurations in the bulk solvent. Successful paths typically cover overall distances of ≈40–60 Å from the protein surface to the flavin C4a carbon and display a stepwise behavior from the time of entrance through the C_2 protein surface (Fig. 1*B*). In fact, O_2 molecules may temporarily reside on the surface (e.g., Fig. 1*B*, step A) and generally visit several cavities along each of these paths (e.g., Fig. 1*B*, steps B and C). An example path is depicted in Fig. 2 and available as Movie S1 video online. Additionally, trajectories show O_2 molecules residing transiently in cavities and niches on the protein surface characterized by the presence of Ala and/or Ile hydrophobic residues, an ideal physicochemical environment to host O_2 molecules. These additional paths carrying O_2 molecules inside the protein, but not in proximity of the C4a flavin atom (distance >6 Å) were therefore distinguished from the above mentioned "complete paths" (see also *SI Text*). 350 K simulations confirm the location of these paths (15 and 25 corresponding events, respectively; data not shown). The relatively limited number of complete paths observed might be, in part, dependent on the 30-ns overall sampling considered (13% of O_2 molecules are inside the protein matrix at the end of our runs at 300 K; 27% at 350 K). However, we stress that this sampling time was sufficient to capture a multitude of diffusion paths.

The observed spontaneous O_2 diffusion matches a model consisting of multiple diffusion paths converging toward residues Phe-270 and Phe-266, in front of the *re*-side of the reduced $FMNH^-$ cofactor (Fig. 3 and Scheme 1). Once O_2 molecules reach Phe-266 and Phe-270 (Fig. 1*B*, step C), transient fluctuations of these aromatic side chains allow O_2 to further diffuse into a smaller cavity defined by flavin C4a, His-396, Phe-266, and Phe-270 (Fig. 1*B*, step D). The side chain of His-396 was proposed to facilitate formation of the C4a-hydroperoxide intermediate (31) and our MD simulations are consistent with the hypothesized role of this preorganized oxygen cavity for C4a-intermediate stabilization. Moreover, they also show that this preorganized cavity is characterized by remarkable side chain

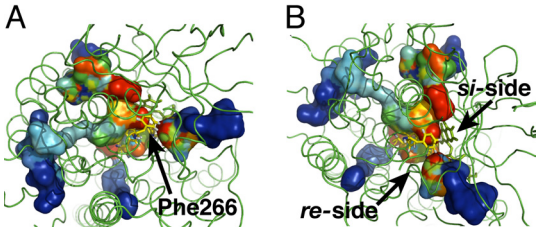

Fig. 3. Funnel-shaped multiple pathways for C_2. (*A*) Time-dependent representation of the 4 complete paths observed from simulations at 300 K converging in front of Phe-266 (top view). (*B*) All pathways conduct O_2 molecules to the flavin *re*-side (side view). Volume isosurfaces are colored depending on simulation time from blue (entrance into the protein) to red (end of successful path).

flexibility, a prerequisite of O_2 diffusion toward the active site (Fig. 2).

Computational predictions and our model for protein-guided O_2 diffusion were validated by combining site-directed mutagenesis and rapid kinetics experiments. Reactions of C_2-FMNH$^-$ with O_2 to form a C4a-hydroperoxyflavin intermediate were monitored using a stopped-flow spectrophotometer (Figs. S2–S4). The kinetics were comparatively investigated in the wild-type protein (35) and in 4 mutants that target Phe-266, the residue suggested by the MD simulations to represent the entry point for the O_2 access to the reactive C4a locus of the flavin ring. The main results of this kinetic analysis were the following (Table 1): (*i*) Binding of the *p*-hydroxyphenylacetate (HPA) substrate to the wild-type C_2-FMNH$^-$ complex causes a 20-fold reduction in the rate of formation of the C4a-hydroperoxyflavin intermediate; (*ii*) mutation of Phe-266 with a bulky Trp side chain causes a very similar drop in rate of the oxygen reaction; and (*iii*) replacement of Phe-266 with smaller side chains (Phe266Pro, Phe266Gly, and Phe266Ala) has little (<5-fold) effect on C4a-hydroperoxyflavin formation, indicating that these mutants retain the ability to efficiently react with oxygen.

Correlating the kinetics with the mechanism of oxygen diffusion is especially difficult because the measured rates of the oxygen reaction and C4a-hydroperoxyflavin formation are composite parameters that result from the rates of oxygen diffusion through the protein matrix and of the chemical steps along the electron-transfer reaction between the oxygen and reduced flavin. Bearing in mind this inherent difficulty in data interpretation, we envision the following working model. O_2 diffusion trajectories converge to Phe-266, at the entrance of the oxygen cavity in front of the flavin C4a atom (Figs. 1 and 2). As shown by the crystal structures, HPA binding involves a conformational change of Phe-266, which must rotate away to make room for the substrate (see Fig. S1 and ref. 31). As a result, substrate binding makes the protein matrix more tightly packed, limiting the conformational fluctuations in the active site. A similar effect is likely to be exerted by the Trp side chain of the Phe266Trp mutant. Consistently, binding of HPA in the wild-type C_2-FMNH$^-$ enzyme and the Trp side chain of the Phe266Trp enzyme decrease the rate of O_2 diffusion, slowing down the overall rate of C4a-hydroperoxyflavin formation (Table 1) (35). This limiting effect is not observed in the proteins in which Phe-266 is replaced by smaller side chains (Phe266Pro, Phe266Gly, and Phe266Ala). The differences between the rate constants of these mutants and of the wild-type enzyme are likely to reflect the increased solvent accessibility of the oxygen cavity as indicated by the lower hydroxylation ratio (i.e., product formed/FMNH$^-$ used) exhibited by the Phe266Gly protein compared with the wild type (62 ± 5% vs. 89 ± 3%) (see *SI Text*) (3, 31, 36). Moreover, it must be noted that the mutants can bind HPA only after formation of the hydroperoxyflavin intermediate and, therefore, their oxygen reaction rates are not affected by HPA binding, differently from the wild-type enzyme (Table 1).

To further validate the O_2 diffusion model obtained from MD simulations, we constructed the C_2(Tyr296Phe) mutant that targets a residue close to the reactive site of the flavin whereas it is not part of the predicted diffusion paths. This mutant reacts with O_2 identically to the wild-type enzyme; the C4a-hydroperoxyflavin is formed with rate constants of 1.2×10^6 and 4.0×10^4 $M^{-1}{\cdot}s^{-1}$ in absence and presence of HPA, respectively (Table 1). These values are essentially the same as those of the wild-type enzyme and confirm that Tyr-296 is not part of any O_2 diffusion path as predicted by our simulations.

Table 1. Reoxidation rates for reduced C_2(mutant)-FMNH$^-$ with O_2 in presence/absence of HPA

	Rate constants of formation of C4a-hydroperoxy FMN, 10^4 $M^{-1}{\cdot}s^{-1}$	
Mutants	−HPA	+HPA
Wild-type	110	4.8
Phe266Gly*	15	16
Phe266Ala*	20	19
Phe266Pro*	14	17
Phe266Trp*	4.8	4.6
Tyr296Phe	120	4.0

+HPA, reaction of C_2(mutant)-FMNH$^-$ with O_2 in presence of HPA. −HPA, reaction of C_2(mutant)-FMNH$^-$ with O_2 in absence of HPA.

*Differently from the wild-type, HPA does not affect the oxygen reactivity of the four Phe266 mutants which bind HPA only after reaction with O_2 and formation of C4a-hydroperoxyflavin (see Figs. S3 and S4).

Oxygen Diffusion into AldO. O_2 diffusion into an oxidase was addressed for AldO, a soluble monomeric flavoprotein of the class of vanillyl-alcohol oxidase, which contains a covalently bound FAD cofactor (32, 37). AldO catalyzes a typical 2-electron flavin-mediated oxidation of a terminal C-OH moiety of a polyol substrate to the corresponding aldehyde, with the concomitant reduction of the flavin cofactor. The reduced flavin (FADH$^-$) then reacts with O_2 to form H_2O_2, which completes the catalytic cycle. Because its crystal structure has been solved at high resolution (1.1 Å) (32) and the kinetic mechanism has been established by presteady state kinetic analyses (37), AldO serves as an excellent oxidase prototype.

Enhanced-statistics MD simulations were initialized based on the 3-dimensional structure of FADH$^-$-complexed AldO and extended for 50 ns of overall enhanced-time (Table S1). These simulations were set-up to capture O_2 diffusion before FADH$^-$ oxidation. Out of a total of 500 O_2 trajectories at 300 K, we observe 5 complete spontaneous diffusion pathways that bring O_2 molecules in front of the isoalloxazine ring of the FADH$^-$ cofactor (Fig. 4), starting from random configurations in the bulk solvent. Simulations at 350 K confirm the location of these successful paths (22 events; data not shown). Several O_2 molecules that initially reside in cavities on the protein surface subsequently diffuse into the AldO interior (e.g., Fig. 4*B*, steps A, B, D, F, and H). As observed in the C_2 monooxygenase system, these surface cavities typically display at least one hydrophobic residue, such as Ala and/or Ile. A remarkable example is the all-Ala pocket of Ala-88, Ala-91, and Ala-277 used to capture O_2 molecules from the bulk solvent (Fig. S5).

The spontaneous O_2 diffusion into AldO matches a model consisting of multiple diffusion paths converging toward a few key residues neighboring the reactive moiety of the flavin cofactor, similarly to what observed for C_2. All protein-guided diffusion pathways converge into a site defined by Ala-105, Tyr-87, and Thr-120 at ≈6 Å from the *re*-side of FADH$^-$ (Figs. 4 and 5). Once O_2 molecules reach Tyr-87 or Thr-120, they (3

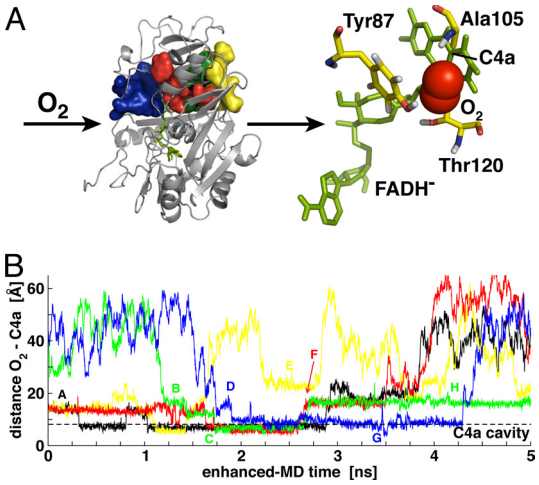

Fig. 4. O_2 spontaneous diffusion into alditol oxidase. (*A*) Five paths are observed at 300 K (volume isosurfaces) (*Left*). All paths conduct O_2 molecules (red spheres) (*Right*) to the *re*-side of the $FADH^-$ reduced flavin cofactor (green sticks). (*B*) Time series of the O_2 – C4a distance for the successful diffusion paths and key steps (see *Oxygen Diffusion into AldO*). The dashed horizontal line defines the C4a flavin cavity.

paths out of 5) eventually proceed to a preorganized cavity defined by flavin C4a and Ala-105, which coincides with the cavity previously proposed based on AldO X-ray structures (32). Thus, the side chain of Ala-105 creates a favorable hydrophobic environment to stabilize the presence of an O_2 molecule next to the reduced flavin (Fig. 4 *A* and *B*, steps C and G). Clearly, protein dynamics is required for the successful diffusion of O_2 molecules to the active site. It is striking to observe that, similar to C_2, all complete diffusion pathways (i.e., all pathways carrying oxygen from the bulk solvent to the flavin cofactor) converge to only one side of the reduced flavin (*re*-side) (Fig. 5 and Scheme 1). Moreover, they all cross only a limited part of the AldO protein structure, i.e., the substrate-domain.

Table 2 summarizes the rapid kinetics experiments for oxygen reactivity of reduced AldO and its Ala-105 mutants. The data show that the rate constant of AldO reoxidation (13×10^4 $M^{-1}{\cdot}s^{-1}$) is hardly affected by the Ala105Ser mutation (14×10^4 $M^{-1}{\cdot}s^{-1}$) whereas the Ala105Gly mutant is somewhat faster (20×10^4 $M^{-1}{\cdot}s^{-1}$) (Fig. S6). Apparently, small changes in the size of the side chain at position 105 have little effect on oxygen reactivity. In this regard, we notice that one would not expect a drastic increase in reactivity with oxygen in the Ala105Gly mutant, because the reaction rate of wild-type AldO is already high and is also limited by other funnel residues and the actual electron-transfer step from O_2 to the flavin (3, 32). All attempts to replace Ala-105 with larger

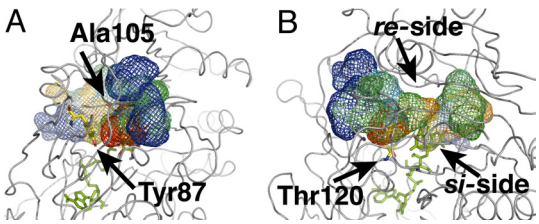

Fig. 5. Funnel-shaped multiple pathways for alditol oxidase. (*A*) Time-dependent representation of 3 complete paths observed from simulations at 300 K converging in close contact with Ala-105 (volume surfaces, top view). (*B*) All pathways conduct O_2 molecules to the flavin *re*-side (side view). For graphical purposes only 3 paths are displayed. Volume isosurfaces are colored depending on simulation time from blue (entrance into the protein) to red (end of successful path).

Table 2. Kinetic parameters for reaction of AldO(mutant)-$FADH^-$ with O_2

Mutants	K_M, mM	k_{cat}, s^{-1}	k_{cat}/K_M, $mM^{-1}{\cdot}s^{-1}$	k_{ox}, 10^4 $M^{-1}{\cdot}s^{-1}$
Wild-type	0.33	11.4	34.5	13
Ala105Gly	1.2	10.2	8.5	20
Ala105Ser	1.8	8.7	4.8	14

The steady state parameters were determined using xylitol as substrate. The k_{ox} reoxidation rate values denote the rate at which $FADH^-$ in AldO is reacting with O_2 evidenced by flavin reoxidation.

side chains failed because the mutants were extremely unstable and/or unable to bind FAD. However, strong support for the role of Ala-105 as O_2 entry point to the active site is provided by recently reported mutagenesis data on plant L-galactono-1,4-lactone dehydrogenase (GALDH) (38), which shares 25% sequence identity with AldO. As a typical dehydrogenase, this enzyme reacts poorly with O_2. However, its oxygen reactivity could be substantially increased (400-fold) to a level comparable to that of typical oxidases by simply mutating Ala-113 (homologous to Ala-105 of AldO) to Gly (38). Apparently, Ala-105 in AldO already allows O_2 access to the reduced FAD whereas in GALDH—due to its specific active site—it needs to be replaced by a smaller residue to allow O_2 to pass through. This finding indicates that, consistently with our MD predictions for AldO, also in GALDH O_2 diffuses and approaches the flavin from the position corresponding to that of AldO Ala-105.

Discussion

We used an integrated computational and experimental procedure, combining X-ray crystallography, enhanced-statistics MD simulations, rapid kinetic experiments, and site-directed mutagenesis to shed light on how O_2 molecules diffuse into the active site of flavoenzymes with different catalytic activity (monooxygenase and oxidase) and folding topologies. In both simulated systems, distinct and multiple protein-guided O_2 diffusion pathways converge toward defined active site entry points, forming funnel architectures. The observation that a specific set of residues form entry sites for the access of oxygen to the flavin cofactor—as Phe-266 in C_2 and Ala-105 in AldO—is consistent with what was recently reported for cholesterol oxidase (12) and sarcosine oxidase (39). However, this does not strictly imply the presence of individual diffusion pathways. Instead, our results suggest that multiple diffusion pathways, converging to a few key residues, are operative and represent a more effective structural model to combine high specificity and high kinetic efficiency in oxygen-using flavoenzymes. From a computational standpoint, we emphasize that in this work, O_2 diffusion was only solvent- or protein-guided—i.e., no biasing force was used to direct the reactants to the protein active sites. We stress, therefore, that a direct picture of the diffusion process at the atomic scale was obtained a priori and only subsequently used as a prediction tool to design the experiments addressing oxygen reactivity.

Our observations are also relevant to the understanding of the reaction mechanism of oxygen with reduced flavin (3, 26). MD simulations indicate that O_2 is able to reach specifically the flavin C4a atom both in the monooxygenase and the oxidase (Figs. 1 and 4). This implies that—independently of the nature of the enzymatic reaction—O_2 would react with the flavin by direct contact with the C4a atom of the cofactor. In this scenario, the C4a atom appears to be the locus directly involved in the electron transfer from the reduced cofactor to O_2, which is consistent with isotope effect studies performed on glucose oxidase (29). The combination of our data with the results obtained by site-directed mutagenesis on various flavoenzymes (38, 39) indicates that the difference among dehydrogenases, monooxygenases, and oxidases ultimately resides in the fine modulation of the local environment embedding the C4a

atom; its accessibility, the distribution of charged and polar groups to favor electron transfer between reduced flavin and O_2, and the extent to which the oxygen cavity is capable of stabilizing the C4a-hydroperoxyflavin.

Methods

Molecular Model and Enhanced-Statistics MD Simulations. Ten MD trajectories of the C_2 homodimer (chain A and D; 798 residues; $FMNH^-$ cofactor; initial model PDB entry 2JBS; 2.8 Å resolution) (31) and 10 trajectories of the AldO monomer (418 residues; $FADH^-$ cofactor; initial model PDB entry 2VFR; 1.1 Å resolution) (32) at 300 and 350 K were generated using the GROMOS05 software for biomolecular simulation (40), the GROMOS 53A6 parameter set (41), and compatible ion parameters (42) and SPC water model (43). A summary is reported in *SI Text* and Table S1. A procedure for enhanced-statistics MD simulation was used for O_2 spontaneous diffusion. It involves (*i*) reduced masses (1.6 u) for the oxygen atoms in the O_2 molecules (21); (*ii*) enhanced statistics from 100 (independent and noninteracting) O_2 molecules in the system, kept beyond a minimum pair distance by a network of repulsive half-harmonic distance-restraining potentials during the equilibration phase (to avoid biasing their initial location before diffusion); (*iii*) a fast grid-based pairlist-construction algorithm (44) as implemented in the GROMOS05 MD++ module (40); (*iv*) enhanced statistics from 10 independent MD runs at 300 and 350 K. O_2 diffusion statistics were collected over a total of 10 independent trajectories of systems with 100 O_2 molecules each, monitored for a total enhanced-MD time of 30 (C_2) or 50 (AldO) ns. The rather high O_2 apparent concentrations (C_2: ≈0.14 M or AldO: ≈0.3 M; for comparison, an O_2 saturated buffer is ≈1.2 mM) allow capturing a sufficient statistics of O_2-protein encounter events without perturbing protein overall structure at both 300 and 350 K. RMSD time series of C_2 and AldO backbone C^α-atoms are reported in Figs. S7 and S8, together with computational details. The term ''enhanced-MD time'' points out that, the kinetic properties of simulated O_2 molecules differ from standard MD simulation. Computer simulations were used to predict the location of oxygen diffusion pathways along C_2 and AldO configurational distributions; instead, kinetic properties were measured by experiments. The term ''enhanced-statistics'' emphasizes that an improved statistics is achieved compared with standard MD simulation. No biasing force or potential is used to bring O_2 molecules inside the enzyme active sites. Instead, O_2 freely diffuses on the free-energy landscape starting from a nonarbitrary configuration and spontaneously reaches the preorganized cavities described in the text. The Pymol (45) and VMD (46) software packages were used for graphical representations.

Rapid Kinetics and Oxygen Reactivity. *C_2.* Rapid kinetics measurements were performed at 277 K with a Hi-Tech Scientific Model SF-61DX stopped-flow spectrophotometer in single- or double-mixing mode (observation cell optical path-length of 1 cm). The stopped-flow instrument was maintained under anaerobic conditions by flushing the flow system with an O_2 scrubbing solution consisting of 400 μM glucose, 1 mg·ml^{-1} glucose oxidase (15.5 units per ml), and 4.8 μg·ml^{-1} catalase in 50 mM sodium phosphate buffer pH 7.0. The O_2 scrubbing solution was left in the flow system overnight and was thoroughly rinsed with anaerobic buffer before experiments. To study the reaction of C_2 mutants with O_2, the reduced enzyme in presence and absence of substrate (HPA) in 50 mM sodium phosphate buffer pH 7.0 was prepared according to the protocol used for the wild-type enzyme (35), followed by mixing with buffers of different O_2 concentrations. Apparent rate constants (k_{obs}) from kinetic traces were calculated from exponential fits using the KineAsyst3 (Hi-Tech Scientific) or Program A (R. Chang, J.-y. Chiu, J. Dinverno, and D.P. Ballou, University of Michigan, Ann Arbor, MI) software packages. Rate constants were obtained by a Levenberg-Marquardt nonlinear fit of k_{obs} versus O_2 concentrations, as implemented in the KaleidaGraph software (35). *SI Text* reports experimental details.

AldO. Purified mutant and wild-type AldO were obtained as described in ref. 37. Rapid kinetics measurements were performed using an Applied Photophysics stopped-flow apparatus model SX17MV following methods reported in ref. 37. Reduced AldO was obtained by anaerobic dithionite reduction. All experiments were performed at 300 K and in a 50 mM potassium phosphate buffer pH 7.5. Experimental details are reported in *SI Text*.

ACKNOWLEDGMENTS. This work was supported by the National Science Foundation Grant PHY-0822283; the National Institutes of Health and National Science Foundation (R.B. and J.A.M.); the Howard Hughes Medical Institute (J.A.M.); the American Chemical Society Petroleum Research Fund Grant 46271-C4 and Ministero dell'Istruzione, dell'Università e della Ricerca (A.M.); the EU-FP7 ''Oxygreen'' project (A.M. and M.W.F.); the Carbohydrate Research Center Wageningen (to W.J.H.v.B.); the Thailand Research Fund grant BRG5180002 and the Faculty of Science, Mahidol University (P. Chaiyen); the Institute for the Promotion of Teaching Science and Technology (P. Chenprakhon); Royal Golden Jubilee PhD Program Grant PHD/0008/2549 (to K.T.); the Dutch Technology Foundation Stichting Technische Wetenschappen Grant 7726, the Nederlandse Organisatie voor Wetenschappelijk Onderzoek applied science division, and the Technology Program of the Ministry of Economic Affairs (R.T.W.) We thank the Center for Theoretical Biological Physics for the computing resources.

1. Que L Jr, Tolman WB (2008) Biologically inspired oxidation catalysis. *Nature* 455:333–340.
2. Perutz MF (1979) Regulation of oxygen affinity of hemoglobin: Influence of structure of the globin on the heme iron. *Annu Rev Biochem* 48:327–386.
3. Massey V (1994) Activation of molecular oxygen by flavins and flavoproteins. *J Biol Chem* 269:22459–22462.
4. Zou S, Baskin JS, Zewail AH (2002) Molecular recognition of oxygen by protein mimics: Dynamics on the femtosecond to microsecond time scale. *Proc Natl Acad Sci USA* 99:9625–9630.
5. Calhoun DB, Vanderkooi JM, Woodrow GV III, Englander SW (1983) Penetration of dioxygen into proteins studied by quenching of phosphorescence and fluorescence. *Biochemistry* 22:1526–1532.
6. Calhoun DB, Vanderkooi JM, Englander SW (1983) Penetration of small molecules into proteins studied by quenching of phosphorescence and fluorescence. *Biochemistry* 22:1533–1539.
7. Johnson BJ, et al. (2007) Exploring molecular oxygen pathways in Hansenula polymorpha copper-containing amine oxidase. *J Biol Chem* 282:17767–17776.
8. Saam J, Ivanov I, Walther M, Holzhutter HG, Kuhn H (2007) Molecular dioxygen enters the active site of 12/15-lipoxygenase via dynamic oxygen access channels. *Proc Natl Acad Sci USA*:13319–13324.
9. Chen L, Lyubimov AY, Brammer L, Vrielink A, Sampson NS (2008) The Binding and release of oxygen and hydrogen peroxide are directed by a hydrophobic tunnel in cholesterol oxidase. *Biochemistry*:5368–5377.
10. Koutsoupakis K, Stavrakis S, Soulimane T, Varotsis C (2003) Oxygen-linked equilibrium CuB-CO species in cytochrome ba3 oxidase from Thermus thermophilus. Implications for an oxygen channel ar the CuB site. *J Biol Chem* 278:14893–14896.
11. Lario PI, Sampson N, Vrielink A (2003) Sub-atomic resolution crystal structure of cholesterol oxidase: What atomic resolution crystallography reveals about enzyme mechanism and the role of the FAD cofactor in redox activity. *J Mol Biol* 326:1635–1650.
12. Piubelli L, et al. (2008) On the oxygen reactivity of flavoprotein oxidases: An oxygen access tunnel and gate in Brevibacterium sterolicum cholesterol oxidase. *J Biol Chem*:24738–24747.
13. Riistama S, et al. (1996) Channelling of dioxygen into the respiratory enzyme. *Biochim Biophys Acta* 1275(1–2):1–4.
14. Elber R, Karplus M (1990) Enhanced sampling in molecular dynamics: Use of the time-dependent hartree approximation for a simulation of carbon monoxide diffusion through myoglobin. *J Am Chem Soc* 112:9161–9175.
15. Lakowicz JR, Weber G (1973) Quenching of fluorescence by oxygen. A probe for structural fluctuations in macromolecules. *Biochemistry* 12:4161–4170.
16. Jameson DM, Gratton E, Weber G, Alpert B (1984) Oxygen distribution and migration within Mbdes Fe and Hbdes Fe. Multifrequency phase and modulation fluorometry study. *Biophys J* 45:795–803.
17. Chu K, et al. (2000) Structure of a ligand-binding intermediate in wild-type carbonmonoxy myoglobin. *Nature* 403:921–923.
18. Widboom PF, Fielding EN, Liu Y, Bruner SD (2007) Structural basis for cofactor-independent dioxygenation in vancomycin biosynthesis. *Nature* 447:342–345.
19. Schotte F, et al. (2003) Watching a protein as it functions with 150-ps time-resolved X-ray crystallography. *Science* 300:1944–1947.
20. Koder RL, et al. (2009) Design and engineering of an O(2) transport protein. *Nature* 458:305–309.
21. Hofacker I, Schulten K (1998) Oxygen and proton pathways in cytochrome c oxidase. *Proteins* 30:100–107.
22. Cohen J, et al. (2005) Molecular dynamics and experimental investigation of H_2 and O_2 diffusion in [Fe]-hydrogenase. *Biochem Soc Trans* 33(Pt 1):80–82.
23. Cohen J, Kim K, King P, Seibert M, Schulten K (2005) Finding gas diffusion pathways in proteins: Application to O_2 and H_2 transport in CpI [FeFe]-hydrogenase and the role of packing defects. *Structure* 13:1321–1329.
24. Masgrau L, et al. (2006) Atomic description of an enzyme reaction dominated by proton tunneling. *Science* 312:237–241.
25. Hummer G, Schotte F, Anfinrud PA (2004) Unveiling functional protein motions with picosecond X-ray crystallography and molecular dynamics simulations. *Proc Natl Acad Sci USA* 101:15330–15334.
26. Mattevi A (2006) To be or not to be an oxidase: Challenging the oxygen reactivity of flavoenzymes. *Trends Biochem Sci* 31:276–283.
27. Massey V (1995) Introduction: Flavoprotein structure and mechanism. *FASEB J* 9:473–475.
28. Sucharitakul J, Prongjit M, Haltrich D, Chaiyen P (2008) Detection of a C4a-hydroperoxyflavin intermediate in the reaction of a flavoprotein oxidase. *Biochemistry* 47:8485–8490.
29. Roth JP, et al. (2004) Oxygen isotope effects on electron transfer to O_2 probed using chemically modified flavins bound to glucose oxidase. *J Am Chem Soc* 126:15120–15131.
30. Pau MY, Lipscomb JD, Solomon EI (2007) Substrate activation for O2 reactions by oxidized metal centers in biology. *Proc Natl Acad Sci USA* 104:18355–18362.

31. Alfieri A, et al. (2007) Structure of the monooxygenase component of a two-component flavoprotein monooxygenase. *Proc Natl Acad Sci USA* 104:1177–1182.
32. Forneris F, et al. (2008) Structural analysis of the catalytic mechanism and stereoselectivity in Streptomyces coelicolor alditol oxidase. *Biochemistry* 47:978–985.
33. Adcock SA, McCammon JA (2006) Molecular dynamics: Survey of methods for simulating the activity of proteins. *Chem Rev* 106:1589–1615.
34. van Gunsteren WF, et al. (2006) Biomolecular modeling: Goals, problems, perspectives. *Angew Chem Int Ed Engl* 45:4064–4092.
35. Sucharitakul J, Chaiyen P, Entsch B, Ballou DP (2006) Kinetic mechanisms of the oxygenase from a two-component enzyme, p-hydroxyphenylacetate 3-hydroxylase from Acinetobacter baumannii. *J Biol Chem* 281:17044–17053.
36. Entsch B, Cole LJ, Ballou DP (2005) Protein dynamics and electrostatics in the function of p-hydroxybenzoate hydroxylase. *Arch Biochem Biophys* 433:297–311.
37. Heuts DP, van Hellemond EW, Janssen DB, Fraaije MW (2007) Discovery, characterization, and kinetic analysis of an alditol oxidase from Streptomyces coelicolor. *J Biol Chem* 282:20283–20291.
38. Leferink NG, et al. (2009) Identification of a gatekeeper residue that prevents dehydrogenases from acting as oxidases. *J Biol Chem* 284:4392–4397.
39. Zhao G, Bruckner RC, Jorns MS (2008) Identification of the oxygen activation site in monomeric sarcosine oxidase: Role of Lys265 in catalysis. *Biochemistry* 47:9124–9135.
40. Christen M, et al. (2005) The GROMOS software for biomolecular simulation: GROMOS05. *J Comput Chem* 26:1719–1751.
41. Oostenbrink C, Villa A, Mark AE, van Gunsteren WF (2004) A biomolecular force field based on the free enthalpy of hydration and solvation: The GROMOS force-field parameter sets 53A5 and 53A6. *J Comput Chem* 25:1656–1676.
42. Åqvist J (1990) Ion Water Interaction Potentials Derived from Free-Energy Perturbation Simulations. *J Phys Chem* 94:8021–8024.
43. Berendsen HJC (1981) *Interaction Models for Water in Relation to Protein Hydration* (Pullman, Dordrecht, The Netherlands).
44. Heinz TN, Hünenberger PH (2004) A fast pairlist-construction algorithm for molecular simulations under periodic boundary conditions. *J Comput Chem* 25:1474–1486.
45. De Lano WL (2002) Pymol (DeLano Scientific, Palo Alto, CA).
46. Humphrey W, Dalke A, Schulten K (1996) VMD: Visual molecular dynamics. *J Mol Graphics* 14:33- 38:27–38.